High-level studies of the ionic states of norbornadiene and quadricyclane, including analysis of new experimental photoelectron spectra by configuration interaction and coupled cluster calculations

Michael H. Palmer, Marcello Coreno, Monica de Simone, Cesare Grazioli, R. Alan Aitken, Søren Vrønning Hoffmann, Nykola C. Jones, and Coralyse Peureux

View Online   **Export Citation**   **CrossMark**

ARTICLES YOU MAY BE INTERESTED IN

High-level studies of the ionic states of norbornadiene and quadricyclane, including analysis of new experimental photoelectron spectra by configuration interaction and coupled cluster calculations

Michael H. Palmer,[1,a] Marcello Coreno,[2,b] Monica de Simone,[3,b] Cesare Grazioli,[3,b]
R. Alan Aitken,[4,b] Søren Vrønning Hoffmann,[5,b] Nykola C. Jones,[5,b] and Coralyse Peureux[4,b]

AFFILIATIONS

[1] School of Chemistry, University of Edinburgh, Joseph Black Building, David Brewster Road, Edinburgh EH9 3FJ, Scotland, United Kingdom
[2] ISM-CNR, Istituto di Struttura Della Materia, LD2 Unit, 34149 Trieste, Italy
[3] IOM-CNR Laboratorio TASC, Trieste, Italy
[4] School of Chemistry, University of St Andrews, North Haugh, St Andrews, Fife KY16 9ST, Scotland, United Kingdom
[5] ISA, Department of Physics and Astronomy, Aarhus University, Ny Munkegade 120, DK-8000 Aarhus C, Denmark

[a] Author to whom correspondence should be addressed: m.h.palmer@ed.ac.uk
[b] Electronic addresses: marcello.coreno@elettra.eu, desimone@iom.cnr.it, grazioli@ism.cnr.it, raa@st-andrews.ac.uk, vronning@phys.au.dk, nykj@phys.au.dk, and coralyse.peureux@laposte.net

ABSTRACT

Synchrotron-based photoelectron spectra (PES) of norbornadiene (NBD) and quadricyclane (QC) differ significantly from those in previous studies. The adiabatic ionization energy (AIE_1) for NBD, assigned to the $^2B_1$ state at 8.279 eV, shows a progression of 18 members with decreasing vibration frequency from 390 cm^{-1} to 340 cm^{-1}; our calculated frequency is 381 cm^{-1}. Similarly, the AIE_1 for QC at 7.671 eV, assigned to the $^2B_2$ state, discloses a vibrational progression of nine or more members with vibration frequency decreasing from 703 cm^{-1} to 660 cm^{-1}; our calculated vibration frequency is 663 cm^{-1}. These AIEs, determined by coupled cluster and fourth order Møller–Plesset perturbation theory, were very similar to the corresponding second order perturbation theory results. The calculated AIE symmetry sequences are $^2B_1 < {}^2A_1 < {}^2A_2 < {}^2B_2$ for NBD and $^2B_2 < {}^2A_2 < {}^2B_1 < {}^2A_1$ for QC. The overall PES vertical ionization energy profiles for both compounds were closely reproduced by Tamm–Dancoff approximation energies and intensities. The vibrational structure of the ionic states, determined using Franck–Condon methods, gave a good account of the observed spectra, but the observed envelopes for both IE_1 are complex sets of vibrations, rather than single progressions. The NMR spectra for QC showed residual second order properties at 300 MHz; both QC and NBD have been theoretically analyzed in greater detail using $AA'BB'CC'XX'$ spectra, where all H are coupled; the magnetic shielding and spin–spin coupling constants obtained are similar to experimental values.

I. INTRODUCTION

Recently, we reported new high-resolution photoelectron spectra (PES) of cyclooctatetraene (C_8H_8, COT)[1] and cycloheptatriene (C_7H_8, CHT).[2] These were analyzed in considerable detail by using a combination of Møller–Plesset fourth order perturbation theory, which included single, double, and quadruple substitutions [MP4(SDQ)], configuration interaction (CI), multi-configuration

self-consistent field (MCSCF), and density functional theoretical (DFT) methods.[1,2] These studies were followed by detailed analyses of new vacuum ultraviolet (VUV) absorption spectra for both compounds using closely related theoretical methods.[3,4]

We now present new synchrotron based PES for both norbornadiene (NBD) and quadricyclane (QC). Interconversions between NBD and QC are important in two potentially industrial and commercial applications that are noted below. The present compounds lack conjugated double bonds, as shown in Fig. 1, but are isoelectronic with CHT.

One application of the NBD + QC binary system enables solar energy storage in a single molecular system.[5–8] Another application is as a switch for an optical memory system.[9,10] NBD is converted to its valence isomer QC via an endothermic photoinduced [2 + 2] reversible cycloaddition.[11] Thermal or catalytic induction leads to the reverse reaction, where QC regenerates NBD with release of

heat. When triplet sensitized using acetophenone, the NBD process appears to involve the two triplets, ^{3}NBD and ^{3}QC, followed by relaxation to QC,[12] but not all sensitizers behave similarly. During the NBD $\leftrightarrows$ QC process, up to 100 kJ/mol of chemical energy is stored, a value comparable to contemporary batteries.[13] The main wavelengths of sunlight lie between 300 nm and 700 nm. Since the NBD UV onset is 267 nm, a combination of donor and acceptor groups in the NBD + QC system is necessary to give an improved solar spectrum match; examples have been reported with an onset of absorption up to 529 nm.[11,14,15]

When NBD or its derivatives are converted to the corresponding QC on irradiation, the "OFF" form of the photo-switch occurs. Conversion back to the NBD gives the "ON" form of the switch. In order to release the stored energy as electricity, the photo-switch must interact with a semiconducting electrode surface.[13]

The technological aspects of the NBD $\leftrightarrows$ QC equilibrium lie outside the scope of the current paper, but the electronic states of the neutral and ionic states for the parent molecules of NBD and QC are crucial to understanding these more complex interactions; our work is directed to performing this at a more rigorous level than is currently available. As with CHT and COT previously, the VUV spectra of NBD and QC will be presented in a following paper, which will analyze the VUV spectra in a detailed manner.

For both title compounds, we have determined the lowest observed adiabatic ionization energies (AIEs) of each symmetry using calculations at both the coupled cluster level, including single, double, and quadruple excitations and non-iterative triples [CCSD(T)], and MP4(SDQ) level. We will show that the results for these two hydrocarbons as the basis set is changed are very similar and also to those at the MP2 level. The profiles of both photoelectron spectra will be interpreted up to about 20 eV by the Tamm–Dancoff approximation (TDA), a single excitation configuration interaction (CI) method. Franck–Condon (FC) analyses will be performed on the vibrational structure of several ionic states in each series.

During the synthetic phase of the investigation, it became clear that the ^{1}H NMR spectrum of QC, previously studied at lower frequencies, such as 60 MHz, was incompatible with those at 300 MHz. The change in the appearance of the spectra is considerable since the three-membered rings of QC lead to nearly degenerate ^{1}H NMR signals at low frequencies and hence uncertainty in assignment. Furthermore, the NMR spectra of QC even at 300 MHz showed additional line splitting, arising from second order effects. Since previous study of QC had only been analyzed by first order methods, a full theoretical second order analysis, under conditions where all spin–spin interactions are included, was performed.

Previous work has shown that the PES of NBD and QC are distinct in the gas phase.[16–21] Similarly, chemically induced dynamic nuclear polarization (CIDNP), following chloranil photosensitization, confirms the difference in solution. Electron spin resonance (ESR) spectra and equilibrium structure calculations indicate symmetrical but clearly different structures for the NBD and QC radical cations.[22–25] Much of the early experimental ionization data and theoretical interpretations for NBS and QC are summarized in the National Institute of Standards and Technology (NIST) webbook.[26]
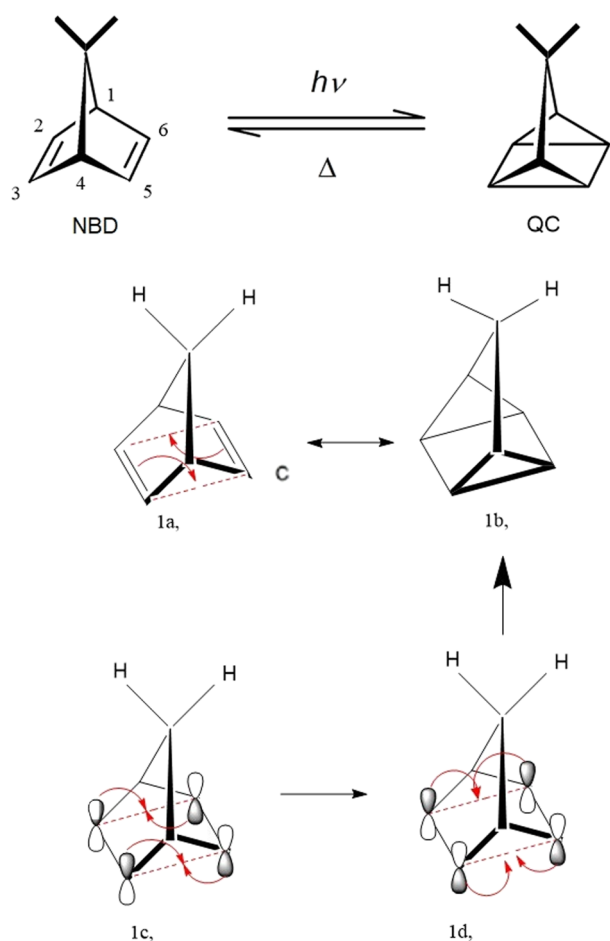
FIG. 1. The compounds (a) norbornadiene (NBD) and (b) quadricyclane (QC). The classical bond switching between the two systems occurs during UV excitation. Rotation of the orbitals toward each other leads to closure to the double cyclopropane system of QC: (c) HOMO and (d) LUMO.

II. METHODS

NBD has CAS Registry No. 121-46-0 and systematic name bicyclo[2.2.1]hepta-2,5-diene. QC has CAS Registry No. 278-06-8, where it is named tetracyclo[2.2.1.0^{2,6}.0$^{3.5}$]heptane. This systematic numbering leads to both NBD and QC having a 7-CH$_2$ group, which enables us to retain the relationship between both compounds. However, an alternative IUPAC nomenclature names QC as tetracyclo[3.2.0.0^{2,7}.0^{4,6}]heptane, which leads to a 3-CH$_2$ group; this difference to NBD is inconvenient and we adopt the 7-CH$_2$ group labeling.

A commercial sample of NBD from Sigma-Aldrich was used after detailed ^{1}H NMR analysis. We found that the chemical shifts and spin coupling constants previously reported[27–31] at 60 MHz and 100 MHz for NBD accurately reproduced the 300 MHz ^{1}H NMR spectrum, but this was not the case for QC, as discussed below.

A. Synthetic methods

QC was prepared from NBD by irradiation using a water-cooled 400 W medium-pressure mercury discharge lamp[32] with acetophenone as a photosensitizer.[33] Fractional distillation of the reactant mixture gave QC but was contaminated by ~5% unchanged NBD. This sample was used in the spectroscopy below since the signals do not interfere with the spectroscopy. Further details are also given in the supplementary material as SM1. The QC ^{1}H NMR spectrum at 300 MHz showed chemical shifts (δ) at 2.02 (2H, t, J = 1.5 Hz, CH$_2$), 1.48–1.50 (4H, m), and 1.34 ppm–1.38 ppm (2H, m), where "t" and "m" refer to the triplet and multiplet, in agreement with the literature.[34,35] Although ^{13}C–^{1}H coupling constants have previously been reported for QC,[36,37] the new spectrum for QC allowed detailed analysis and determination of additional ^{1}H–^{1}H and ^{13}C–^{1}H coupling constants for the first time.

B. The photoelectron spectra of NBD and QC

These were obtained at room temperature on the gas-phase line of the Elettra synchrotron (Basovizza, near Trieste, Italy) using methods described previously.[1,3] The NBD sample vapor was irradiated at both 30 eV and 95 eV photon energy. The 30 eV spectrum covers the energy range 7.473 eV–16.473 eV with 5670 data points (DPs), separated by 0.001 eV (8 cm^{-1}); this corresponds to a total resolution close to 8.5 meV. A wider NBD scan up to 24.473 eV, also using 30 eV irradiation, contained 10 471 DPs, with a separation of 0.0025 eV (20 cm^{-1}). The 95 eV scan for NBD contained 7500 DPs with a separation of 0.005 eV above 14.428 eV. The PES of QC up to 21.8 eV measured using 30 eV photons contained 9463 DP with a separation of 0.002 eV (16 cm^{-1}). The 30 eV PES for NBD and QC, in the 7.5 eV–22 eV energy range, are super-imposed in Fig. 2; the substantial differences support previous conclusions that the two compounds are distinct in the gas phase. The onset for QC, slightly lower than that for NBD, is unexpected in view of its saturated QC structure.
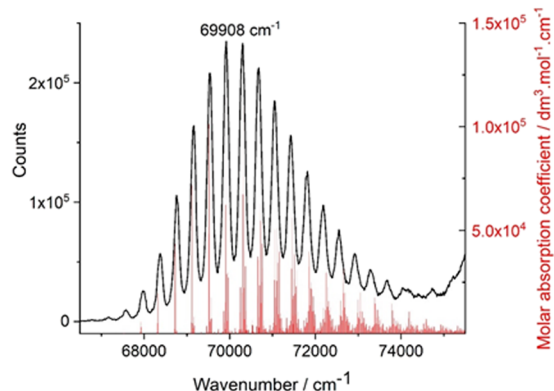
1. Norbornadiene

The expansion of the lowest IE, as in Fig. 3, shows a considerable number of vibrational states, not reported in earlier spectra. It is clear that this band is not a single mode sequence with increasing
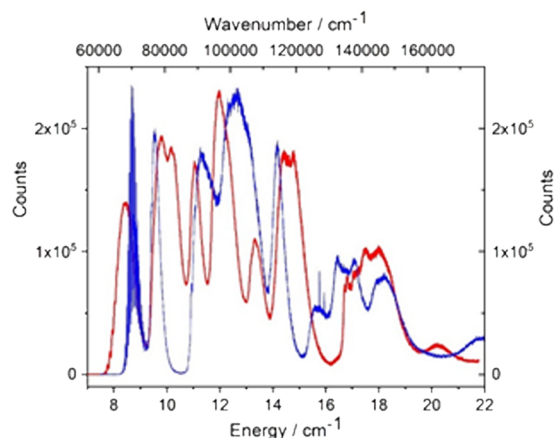
FIG. 2. The photoelectron spectra of norbornadiene (in blue) shown with the quadricyclane spectrum (in red). The onset of the formally saturated hydrocarbon (QC) lies below that for the non-conjugated alkene (NBD).

quanta. Hence, discussion in relation to the neutral state vibrations is irrelevant. This band is discussed in further detail below. The lowest AIE of NBD appears to lie at 8.279 eV. Since the onsets for most of the higher PES bands are not well-defined, these are best described by their vertical ionization energy (VIE). Our NBD analysis by fitting Gaussian peaks to the low-lying ionizations gives a close fit to the observed PES, as shown in Fig. 4. VIE$_2$ shows a shoulder on its leading edge, which we attribute to a group of vibrational states, rather than a separate IE. The fitted peak maxima, which we identify as the VIEs, are discussed below. Further details of the NBD analysis, together with those for QC, are shown in the supplementary material as SM2.

FIG. 3. The lowest ionic state of norbornadiene with vertical ionization energy at 8.6673 eV (69 908 cm^{-1}) is shown in black with the Franck–Condon profile super-imposed in red. Each of the apparent single sequence of vibrational bands is a progressively more complex set of vibrational states as the energy increases. The AIE is probably at 8.2799 eV (66 783 cm^{-1}), the first recognizable member of the initial 392 cm^{-1} sequence.
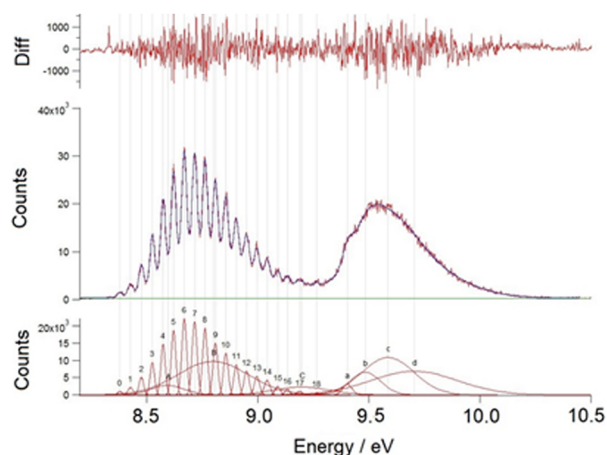
FIG. 4. Detailed analysis of the lowest ionization energy for norbornadiene. The very low levels of residuals (Diff) after fitting are shown in red. Further details of the fit are shown in the supplementary material as SM3.

FIG. 5. Detailed analysis of the lowest ionization energy for quadricyclane using 30 eV irradiation, with an overall resolution of 10 meV; the sample contains ~5% NBD. It is not known whether this represents an equilibrium between the two compounds. The peaks for NBD are marked 12–27. Further details of the fit are shown in the supplementary material as SM3.

2. Quadricyclane

Most of the PES show little evidence of the vibrational structure, but the vibrations shown on the leading edge of AIE_1 are quite different from those on the trailing edge, which are attributed to the small NBD contamination. This is discussed in more detail below. We compare the vibrations on the leading edge with calculated values below, but the spacing of these clearly relates to QC and not NBD. The overall structure of the QC PES lowest IE can best be fit by a group of three asymmetric Gaussian functions, as in Fig. 5.
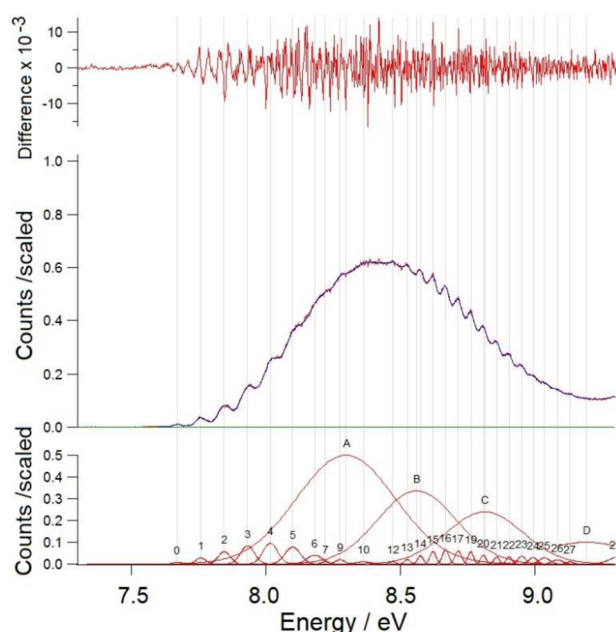
C. Theoretical methods

Our methods have specific uses, and no single suite can lead us to a complete analysis. As in our COT and CHT studies,[1–4] we use several suites.

The equilibrium structures of the X^1A_1 ground states for NBD and QC, shown in the supplementary material under SM5 as scale diagrams, demonstrate the much more compact QC system, arising from the double cyclopropane structure. The atomic coordinates for NBD and QC at the CCSD(T) level are also shown in SM5.

1. Equilibrium structures of the ionic states

Both the GAUSSIAN-16 (G-16)[38] and MOLPRO suites[39–42] were used to determine the AIE and equilibrium structures for the lowest states of each symmetry. The most rigorous procedures adopted here were CCSD(T)[43,44] and MP4(SDQ).[45–47] In contrast to the former method, wave-functions from the latter are readily processed for vibrational analysis by G-16, as described below.

Since these AIE procedures are impracticable for interpretation of the wide scan PES shown in Fig. 2, our approach was to determine the VIE for many states, by means of calculations at the ground state

(X^1A_1) structure, for each of NBD and QC. This broad-brush theoretical approach generates an overall picture of the PES ionic state energies, together with intensities, and was performed by two methods. States where direct ionization occurs from one of the selected sets of DOMOs were formerly termed Koopmans' theorem states (KT), which define $IE_i = −\varepsilon_i$, where ε_i is the orbital energy; this was widely used in early literature on NBD and QC. At higher energy, ionic states are accompanied by simultaneous electronic excitation, often referred to as "shake-up" states. These have vacancies in two occupied orbitals; with one electron distributed between these, the spin between the singly occupied MOs can be either singlet or triplet.

Our most detailed wide scan theoretical approach uses the Tamm–Dancoff approximation (TDA),[48,49] as implemented in GAMESS-UK.[50] It is a Single excitation, Configuration Interaction (CIS) procedure. The CI space was set at 63 active MOs and excludes the seven core molecular orbitals (MOs) in C_{2v} symmetry; it is discussed further below.

We have also been able to determine the adiabatic ionization energies for both NBD and QC in the first (lowest excitation energy) states of each symmetry by using the MP4(SDQ) method. These are also shown below.

2. Vibrational features of the ionic states

The equilibrium structures determined at the MP2 level were processed by the Pisa Group software,[51–53] as implemented in G-16.

3. Basis sets

Those used varied with the nature of the calculation in progress, but all were at least triple zeta valence with polarization (TZVP),[56] 6-311+G[2d,1p],[57] and Def2-TZVPPD.[58] The equilibrium structures were determined using the TZVP and Def2-TZVPPD bases, including the calculations using the CCSD(T) method. The ionic state calculations, including those where vibrational analysis occurred, were at the TZVP level since our related studies reported previously showed this to be adequate. Our present analyses shown in Secs. III C and III D also support this view.

4. NMR chemical shifts

The shielding tensors and the corresponding spin coupling constants were computed with the Gauge-Independent Atomic Orbital (GIAO) method.[54,55] Various studies[54,55] have pointed to the success of the Becke–Lee–Yang–Parr (B3LYP) functional, relative to other density functionals, for the calculation of spin–spin constants in NMR. We have tried several functionals, as shown in the supplementary material, which confirm that B3LYP seems particularly suitable for this purpose.

5. NMR bases

It became clear that to obtain calculated coupling constants close to the experiment, the basis sets should have at least double polarization functions on a triple zeta valence basis set (TZVP); this is normally termed TZ2P. One specifically designed for the prediction of hyperfine coupling tensors of electron paramagnetic resonance (EPR-III) is included;[59,60] it is a triple-zeta basis set including diffuse functions, double d-polarizations, and a single set of f-polarization functions. In addition, the s-functions (6, 2) are contracted to [4, 2] for H and (11, 7, 2, 1)/[7, 4, 2, 1] for C; this results in an improved description close to the nuclei.

At the Hartree–Fock level, the X^1A_1 state doubly occupied orbitals (DOMOs) in the C_{2V} symmetry differ; these are [$10a_1$, $6b_1$, $6b_2$, $3a_2$] for NBD and [$10a_1$, $5b_1$, $7b_2$, $3a_2$] for QC.

III. RESULTS

A. Comparison of the molecular structures of NBD and QC with experimental microwave and other spectral data

Several electron diffraction (ED),[61–63] nematic phase nuclear magnetic resonance (NP-NMR),[64–66] and microwave spectroscopy (MW) papers[67–69] have focused on NBD with few on QC.[70,71] Our theoretical comparisons with these experimental values are generally excellent, which give confidence in the overall theoretical analysis of NBD and QC. Since these results are not central to this study on ionic states, we defer these results to the Appendix, which shows a comparison of the bond lengths, rotational constants (RCs), and quartic centrifugal distortion constants (QCDCs) for neutral NBD in its MW substitution structure,[68] with the present equilibrium structural theoretical values; the latter were determined at both the CCSD(T) and MP4(SDQ) levels, as shown in Appendix, Tables XI and XII.

We find the CCSD(T) energy difference, NBD-QC, at their respective equilibrium structures to be −1.014 eV, close to the previously calculated values[24,72] (−1.023 eV and −1.032 eV, respectively) and experiment.[73]

We use theoretical harmonic frequencies for both NBD and QC considerably in the analyses of the ionic states below. For brevity, we limit these to a_1 modes since these are the only vibrationally active modes present in the PES analyses; full lists of the frequencies, including their variation with ionic state symmetry, are given in the supplementary material as SM6 and can be compared with combined infrared and Raman spectral data for gas, liquid, and polycrystalline phases.[74]

The ionic state RC values determined at the MP4(SDQ) level in Tables XI and XII show some variation with electronic states. For all the C_{2V} states of NBD except $^2A_2$, the double bonds are still apparent, but for the other symmetry states, there is lengthening of bonds with weakening of the CH_2 bridge ($^2A_1$ and $^2B_2$) and breaking of the C=C bonds ($^2A_2$ state). Further details of the structures are given in the supplementary material as SM4. The nodal surfaces for the lowest AIE states of each symmetry are shown in Fig. 6.
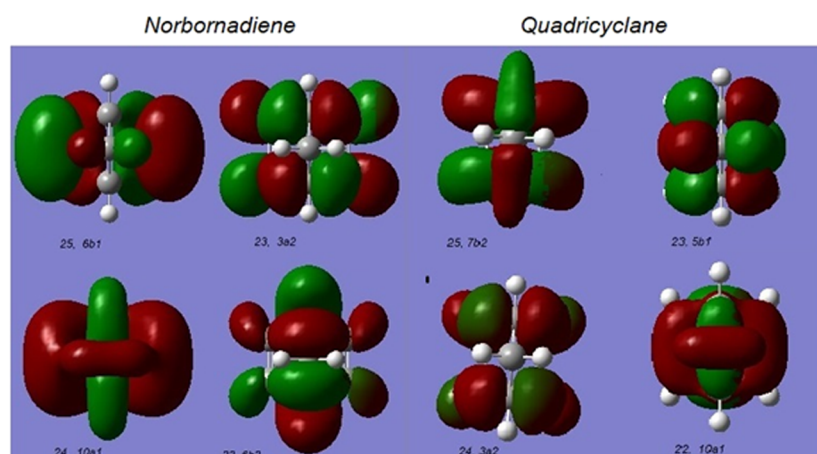
FIG. 6. The highest occupied MOs for NBD and QC with differing sequences by symmetry of the occupied MOs 22–25 (HOMO). There is considerable similarity in the appearance of the electron distribution in both compounds for the a_1 and a_2 symmetry MOs.

B. Reinterpretation of the 1H NMR spectra of QC and NBD

Our experimental spectra for QC are shown in Figs. 7(a)–7(c), with simulations in Figs. 7(d)–7(f); the numerical results are summarized in Table I. The appearance of the QC spectrum is critically dependent upon the ratio (δ_{ab}/J_{ab}) of the coupling constant (J_{ab}) to chemical shift (δ) between a and b. The QC spectra are particularly complex at previously studied frequencies of 60 MHz and 100 MHz[34,36,37] since the nuclei have similar shifts. A previous treatment as an AB_2X_2 spectrum,[34] where A and B were effectively

(A). Experimental 7-CH2 spectrum (ppm)

(D) Simulation

(B). Experimental spectrum (ppm) H2,3,5,6

(E). Simulation

(C). Experimental spectrum H1,4
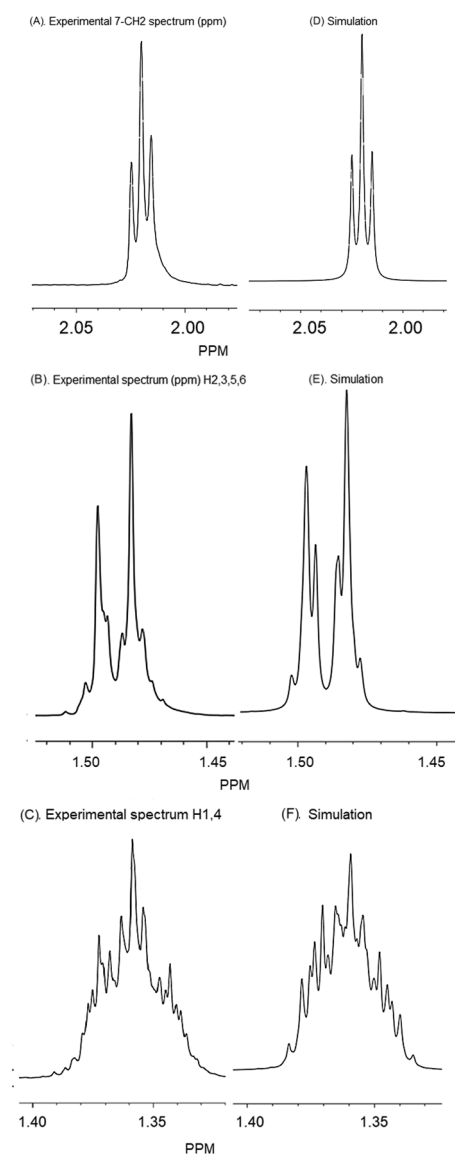
(F). Simulation

FIG. 7. The ^{1}H NMR spectral bands of quadricyclane at 300 MHz [(a)–(c)] with the simulations [(d)–(f)] produced by the assigned coupling constants.

TABLE I. 300 MHz ^{1}H NMR spectral chemical shifts (ppm) and coupling constants (Hz) for both NBD and QC. The only directly comparable environments between NBD and QC are the couplings $J_{1,7}$ and $J_{4,7}$ where the values are similar.

	NBD	QC (present)
δ (1, 4)	3.57	1.360(2)
δ (2, 3, 5, 6)	6.76	1.490(2)
δ (7)	1.98	2.020(2)
$^3J_{1,7} = {}^3J_{4,7}$	1.5	1.5
$^3J_{1,2} = {}^3J_{3,4} = {}^3J_{4,5} = {}^3J_{1,6}$	2.7	4.3
$^3J_{2,3} = {}^3J_{5,6}$	5.0	2.5
$^3J_{2,6} = {}^3J_{3,5}$	0	5.0
$^4J_{1,3} = {}^4J_{2,4} = {}^4J_{4,6} = {}^4J_{1,5}$	1.0	0

degenerate, gave the spectrum as a (uneven) 1:2:1-triplet (A) and a single dominant line with numerous weak bands (B_2).[34] At 300 MHz, the ^{1}H NMR spectrum for QC shows that the multiplicity for the tertiary H-atoms (C_1H/C_4H) is clearly larger than the limiting triple-triplet coupling expected for a first order analysis. Similarly, the uneven intensity of the triplet peaks, notionally 1:2:1 in intensity, also provides evidence that second order effects are still present. Our results for NBD at this level agree with previous analyses, and its spectra are omitted.[31]

We have performed a theoretical analysis using the GIAO approach[56,57] and obtained theoretical chemical shifts and coupling constants for QC. These analyses use an $AA'BB'CC'XX'$ approach where all ^{1}H-nuclei are coupled; XX' are designated as the 7-CH_2 unit because of the larger difference (0.53 ppm) from the other bands that are separated by only 0.13 ppm. Thus, second order spin couplings between chemically equivalent but magnetically non-equivalent atoms (isochronous nuclei)[31] are included. A summary of the comparisons between the experimental NMR results[36,37,71,75] is given in Table I; the theoretical analyses are given in Tables II and III; H-atoms are labeled the attached C-atom. The spin-coupling and chemical shift parameters used in the simulated spectra [Figs. 7(d)–7(f)] reproduce the earlier 60 MHz and 100 MHz spectra satisfactorily. Full arrays for these couplings, together with those for NBD, are shown in the supplementary material at SM2. A subset of the full analysis of the chemical shift and spin coupling constant theoretical analyses is shown in Table I, with additional data in the supplementary material as SM2.

The present calculated chemical shifts for QC, shown in Tables I and II, are in almost exact agreement with those from two ^{2}H and ^{13}C two-dimensional Q-COSY spectral determinations.[71,75] The (1-bond) $^1J_{{}^{13}C^1H}$ spin couplings are very dependent upon both the basis set and the methodology; our best values (unscaled) are within 5% of experiment. Second-order polarization propagator approximations (SOPPAs)[76,77] give even closer values when compared with experiment. Our $^1J_{{}^{13}C^1H}$ values reflect the relative experimental magnitudes, $C_2H > C_1H > C_7H$, as observed. The vicinal ^{1}H–^{1}H couplings $J_{1,2}$ and $J_{2,3}$ are close to experiment, but $J_{2,5}$ and $J_{2,7}$ have not been identified previously; our values are shown in Table III. The calculated ^{1}H–^{1}H couplings values over two- and four-bonds (^2J and ^4J) are all found to be negative, and none are

TABLE II. H- and C-nucleus chemical shift for both QC and NBD calculated by the GIAO method compared with experimental results. The magnetic shielding values are relative to tetramethyl silane (TMS) using the same basis set at its equilibrium geometry. For results from other procedures, see the supplementary material, where the Austin-Frisch-Petersson functional with dispersion (APFD) results are corrected by 0.07 ppm, using our new TMS data as reference nuclei.

QC	Method/centers	H1,4	H2,3,5,6	H7
	Present NMR	1.360	1.490	2.020
	B3LYP/EPR-III	1.33	1.53	2.17
		C1,4	C2,3,5,6	C7
	NMR[35,36]	23.04[35,36]	14.77[3][35,36]	32.03[35,36]
	Q-COSY 2D NMR[71]	22.6	14.4	31.6
	B3LYP/EPR-III	29.08	19.24	38.80
NBD	Method/centers	H1,4	H2,3,5,6	H7
δ from TMS (ppm)	Present + NMR[75]	3.57	6.76	1.98
	B3LYP/EPR-III	3.69	7.28	2.24
		C1/2	C3/4/5/6	C7
	Present NMR	50.215	143.37	75.28
	NMR[75]	50.27	143.42	75.33
	B3LYP/EPR-III	50.78	159.30	87.25

close to zero. Thus, attempts at a first order analysis are of no value for QC.

C. The wide scan PES of NBD and QC

1. Comparison with the theoretical study

The new wide scan spectra, shown in Figs. 8 and 9, have the scaled TDA energies and pole strength intensities superimposed in red; the AIEs determined from the MP4(SDQ) calculations are shown in blue. These calculated sets of AIE and VIE for both compounds are close to the experimental peak onsets and maxima, respectively, as expected. The corresponding unscaled TDA energies for the lower group of PES bands for both compounds are shown in Tables IV and V.

2. Assignment of the PES bands

The two lowest IE of NBD at 8.69 eV and 9.55 eV[18–21] dominated early interest in the spectrum since these previously assigned

TABLE III. ^{1}H^{1}H, ^{13}C^{1}H, and ^{13}C^{13}C spin coupling constants for QC determined by using B3LYP with the EPR-III GIAO method. These are the only unique values, and the chemically equivalent but magnetically non-equivalent values are numerically the same. For results from other procedures, see the supplementary material.

	^{13}C–^{1}H couplings			^{1}H–^{1}H couplings	
Center	B3LYP/ EPR-III	Expt.	Center	B3LYP/ EPR-III	Expt.
CH1	170.00	165.9,[36] 166.0[37]	H1,4	1.20	
C1H4	9.63		H1,2	5.47	4.3
C1H2	−0.26		H1,3	−0.62	
C1H3	0.40		H1,7	1.63	1.5
C1H7	−2.56		H2,3	2.80	2.5
C2H1	1.83		H2,6	6.50	5.0
C2H4	3.65		H2,5	1.50	
C2H2	189.22	183.2,[36] 184.7[37]	H2,7a	−0.34	
C2H3	3.94		H2,7b	−0.34	
C2H6	−2.50		H7a,7b	−11.10	
C2H5	2.71				
C2H7a	0.67				
C2H7b	7.71				
C7H7	133.95	132.2,[36] 131.4[37]			
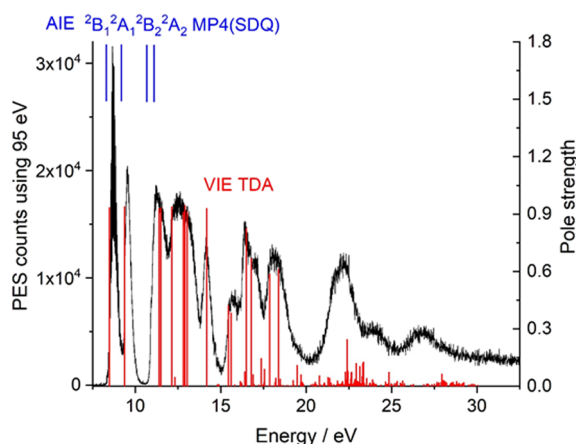
FIG. 8. The wide scan photoelectron spectrum of norbornadiene correlated with the TDA pole strengths (in red). The calculated energies have been fitted to the spectrum by means of a linear correlation where $E_{corr} = 0.912(13) * E_{TDA} +1.067(20)$ with an adjacent R^2 correlation coefficient of 0.998. The MP4(SDQ) AIEs are shown above as blue vertical bars.
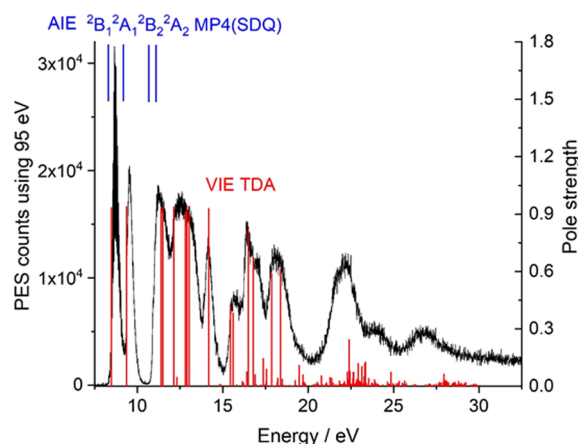
FIG. 9. The wide scan photoelectron spectrum of quadricyclane correlated with the TDA pole strengths. The calculated energies shown in red have been fitted to the spectrum by means of a linear correlation of the energies where $E_{corr} = 0.887(15) * E_{TDA} +1.333(20)$ with an adjacent R^2 correlation coefficient of 0.998. The adiabatic ionization energies for the lowest states of each symmetry calculated by the MP4(SDQ) method are shown in blue.

to π-ionizations were attributed to the symmetric (π^+) and antisymmetric (π^-) combinations of the two π-orbitals with the IE order $^2B_2(\pi^-) < {}^2A_1(\pi^+)$. Although this was attributed to through-space interactions being more important than through-bond interactions,[18] this is the natural energy order owing to the presence of a node in the anti-symmetric combination.[78–80] Although the TDA calculations for both NBD and QC suggest an almost identical

lowest VIE, there is little doubt that the QC PES shows the lower experimental AIE onset; we attribute this to extra σ-bond strain introduced by the double cyclopropane system of QC, some of which is released upon ionization.

Several attempts to assign symmetry to higher VIE for NBD have been made but with little success. Thus, the asymmetry

TABLE IV. The TDA analysis of the ionic states of NBD used for assignment of the NBD photoelectron spectrum. The ionic populations of the vacated MOs are spread over several ionic states at higher energy; only poles greater than 0.02 are shown.

Energy	Symmetry	Pole strength	Orbital vacated	Energy	Symmetry	Pole strength	Orbital vacated
8.199	$^2B_1$	0.9032	$5b_1^{-1}$	17.395	$^2A_1$	0.7409	$4a_1^{-1}$
9.224	$^2A_1$	0.9019	$7a_1^{-1}$	17.783	$^2A_2$	0.0600	$1a_2^{-1}$
11.434	$^2A_2$	0.8971	$2a_2^{-1}$	18.564	$^2A_2$	0.2025	$1a_2^{-1}$
11.550	$^2B_2$	0.9015	$4b_2^{-1}$	18.714	$^2A_2$	0.4434	$1a_2^{-1}$
12.178	$^2B_1$	0.9011	$4b_1^{-1}$	19.025	$^2A_1$	0.2275	$3a_1^{-1}$
12.564	$^2B_2$	0.1671	$3b_2^{-1}$	19.071	$^2A_1$	0.4243	$2a_1^{-1}$
12.815	$^2A_1$	0.8796	$6a_1^{-1}$	19.210	$^2A_2$	0.0227	$1a_2^{-1}$
12.832	$^2B_2$	0.7357	$3b_2^{-1}$	19.471	$^2A_2$	0.0244	$1a_2^{-1}$
13.239	$^2A_1$	0.8568	$5a_1^{-1}$	22.695	$^2A_1$	0.2888	$1a_1^{-1}$
14.286	$^2B_1$	0.8873	$3b_1^{-1}$	23.023	$^2B_2$	0.0404	$1b_2^{-1}$
15.986	$^2B_1$	0.7284	$2b_1^{-1}$	23.241	$^2B_2$	0.0393	$1b_2^{-1}$
16.224	$^2B_1$	0.0642	$2b_1^{-1}$	23.483	$^2B_2$	0.0691	$1b_2^{-1}$
16.949	$^2B_2$	0.3388	$2b_2^{-1}$	23.604	$^2B_2$	0.1374	$1b_2^{-1}$
17.039	$^2B_2$	0.5046	$2b_2^{-1}$	23.718	$^2B_2$	0.0468	$1b_2^{-1}$
17.187	$^2B_1$	0.0423	$2b_1^{-1}$	24.037	$^2B_1$	0.0408	$1b_1^{-1}$

TABLE V. The TDA analysis of the ionic states of QC used for assignment of the QC photoelectron spectrum. The ionic populations of the vacated MOs are spread over several ionic states at higher energy; only poles greater than 0.02 are shown. All $^2A_2$ shake-up states have very low intensity.

Energy	Symmetry	Pole strength	Orbital vacated	Energy	Symmetry	Pole strength	Orbital vacated
8.199	$^2B_2$	0.919 45	$7b_2^{-1}$	19.931	$^2B_2$	0.026 11	$3b_2^{-1}$
9.608	$^2A_2$	0.917 19	$3a_2^{-1}$	20.897	$^2B_1$	0.184 74	$2b_1^{-1}$
9.946	$^2B_1$	0.916 71	$5b_1^{-1}$	21.105	$^2B_1$	0.210 36	$2b_1^{-1}$
10.914	$^2A_1$	0.911 19	$10a_1^{-1}$	21.121	$^2B_1$	0.171 68	$2b_1^{-1}$
11.997	$^2B_1$	0.913 01	$4b_1^{-1}$	21.375	$^2B_1$	0.089 38	$2b_1^{-1}$
12.134	$^2B_2$	0.912 87	$6b_2^{-1}$	22.366	$^2B_1$	0.062 89	$2b_1^{-1}$
13.440	$^2A_1$	0.906 00	$9a_1^{-1}$	23.916	$^2A_1$	0.145 51	$5a_1^{-1}$
14.603	$^2A_1$	0.899 66	$8a_1^{-1}$	24.032	$^2A_1$	0.165 11	$5a_1^{-1}$
14.861	$^2B_1$	0.904 23	$3b_1^{-1}$	24.115	$^2A_1$	0.042 46	$5a_1^{-1}$
14.886	$^2B_2$	0.899 18	$5b_2^{-1}$	25.007	$^2B_2$	0.033 84	$2b_2^{-1}$
17.680	$^2A_2$	0.863 64	$2a_2^{-1}$	25.077	$^2A_1$	0.030 16	$4a_1^{-1}$
17.916	$^2A_1$	0.859 89	$7a_1^{-1}$	25.094	$^2A_1$	0.034 36	$4a_1^{-1}$
18.648	$^2B_2$	0.812 02	$4b_2^{-1}$	25.379	$^2B_2$	0.064 45	$2b_2^{-1}$
19.005	$^2A_1$	0.735 79	$6a_1^{-1}$	25.475	$^2B_2$	0.064 98	$2b_2^{-1}$
19.445	$^2A_1$	0.110 51	$6a_1^{-1}$	25.508	$^2B_2$	0.083 87	$2b_2^{-1}$

parameter (β) in PES angular distribution studies of NBD for these two ionic states was found to be 1.04(1) and 0.94(1) for $^2B_2$ and $^2A_1$ states, respectively;[81,82] but does not confirm these two symmetry assignments. Similarly, irradiation of NBD with He* (2^3S state at 19.82 eV), termed Penning ionization electron spectra (PIES),[20] showed that the second and fourth IEs are more intense than the first and third under PIES relative to direct He(I) (27.211 eV) irradiation, but again this did not lead to experimental identification of any ionic state symmetries. However, both IE$_1$ and IE$_2$ under PIES showed broad shoulders relating to the vibrational structure, which was absent on both the He(I) and He(II) (40.78 eV) spectra.[20]

Although the third and higher IEs of NBD and all of those for QC will relate to σ-ionization, interpretation of the principal band groupings in the envelope and their states is important. Lindholm *et al.*[19] presented the first wide energy range study of the NBD PES using a semi-empirical procedure known as the Spectroscopic Potential adjusted Intermediate Neglect of Differential Overlap (SPINDO). This analysis[19] and that for another closely related method also showed an acceptable interpretation of the experimental groupings of IE; some unpublished details of it[19] (known as HAM3) are reported by Von Niessen and Diercksen.[83] Later, results by small scale singles and doubles configuration interaction (CISD) studies[84] and also Green's function (single excitation (CIS) studies)[83] gave a similar level of agreement with the observed PES. In all cases, the lowest four IEs were $^2B_1 < {}^2A_1 < {}^2A_2 < {}^2B_2$.

There are very few studies of the QC PES,[85,86] and the previous assignment is based upon a Modified Intermediate Neglect of Differential Overlap (MINDO) calculation; the lowest IEs for QC using MINDO were $^2B_2 < {}^2A_2 < {}^2B_1 < {}^2A_1$.

The TDA results in Tables IV and V give a very close fit to the observed PES for both NBD and QC. Although these show

TABLE VI. The a$_1$ harmonic frequencies including their sequence numbers for the ground and ionic states for norbornadiene determined at the TZVP level. The $^2A_1$ calculation leads to a negative b$_2$ eigenvalue (mode 1). The Franck–Condon calculation is performed by projection out from the X^1A_1 modes, the one having the largest overlap with the ionic state in the Duschinsky matrix. The full sequences are shown in the supplementary material as SM6. The modes labeled in ascending frequency are as used in the Franck–Condon profiles of active modes shown in Table VII.

X^1A_1	$^2B_1$	$^2B_2$	$^2A_1$	$^2A_2$
1	2	3	2	4
429	399	429	453	298
7	7	7	5	8
730	782	672	661	746
8	8	8	8	12
794	839	712	787	884
11	11	10	9	14
904	923	796	827	982
16	15	18	15	15
967	1013	969	964	1004
20	19	21	20	22
1138	1132	1110	1151	1227
24	25	25	21	27
1258	1292	1196	1187	1401
29	28	28	27	29
1513	1503	1483	1520	1633
31	30	30	28	30
1615	1537	1619	1563	1917
32	32	33	30	31
3096	3107	2951	3149	3237
35	35	34	32	36
3174	3221	3149	3210	3339
39	38	39	37	38
3277	3264	3289	3279	3369

TABLE VII. Vibrationally excited ionic states of NBD. The modes excited shown here are the a_1 frequencies for the ionic state shown together with the number (n) of quanta excited as "^n." Binary and higher combination bands are separated by semicolons.

Energy cm^{-1}	Modes excited + quanta	Relative intensity	Energy cm^{-1}	Modes excited[a] + quanta	Relative intensity[b]
$^2B_1$ energy of the 0–0 transition: 8.262 4 eV			$^2A_1$ energy of the 0–0 transition: 9.646 8 eV		
0	0	820	0	0	6 877
399	2^1	4 147	453	2^1	24 060
798	2^2	15 900	661	5^1	4 785
1197	2^3	39 500	905	2^2	56 040
1238	8^1; 2^1	1 949	1113	5^1; 2^1	21 160
1596	2^4	71 560	1358	2^3	59 880
1637	8^1; 2^2	7 166	1566	5^1; 2^2	31 830
1995	2^5	100 800	1604	20^1; 2^1	3 329
2036	8^1; 2^3	17 060	1693	8^1; 2^2	2 380
2210	15^1; 2^3	2 327	1732	9^1; 2^2	3 532
2329	19^1; 2^3	4 911	1774	5^2; 2^1	4 893
2335	30^1; 2^2	5 576	1811	2^4	73 830
2394	2^6	115 000	2016	28^1; 2^1	3 467
2435	8^1; 2^4	29 590	2019	5^1; 2^3	49 480
2477	8^2; 2^2	1 969	2057	20^1; 2^2	7 067
$^2B_2$ energy of the 0–0 transition: 10.688 7 eV			$^2A_2$ energy of the 0–0 transition: 11.373 9 eV		
0	0	729	0	0	3616
1196	25^1	2 717	746	7^1	7965
1343	7^2	2 066	1227	21^1	3274
1868	25^1; 7^1	8 230	1492	7^2	7794
2392	25^2	6 302	1630	11^1; 7^1	2706
2540	25^1; 7^2	11 630	1728	13^1; 7^1	4224
2978	25^1; 21^1; 7^1	4 932	1973	21^1; 7^1	6423
3064	25^2; 7^1	18 790	2238	7^3	4491
3211	25^1; 7^3	10 150	2376	11^1; 7^2	2383
3336	25^1; 10^1; 7^2	2 672	2474	13^1; 7^2	6334
3502	25^2; 21^1	2 688	2663	29^1; 7^1	4833
3589	25^3	7 213	2719	21^1; 7^2	5585
3650	25^1; 21^1; 7^2	6 613	2857	21^1; 11^1; 7^1	3295
3736	25^2; 7^2	16 880	2955	21^1; 13^1; 7^1	5686
3860	25^2; 10^1; 7^1	5 025	3200	21^2; 7^1	3613
3883	25^1; 7^4	6 098	3220	13^1; 7^3	3682
4007	25^1; 10^1; 7^3	2 440	3409	29^1; 7^2	6804
4033	25^2; 18^1; 7^1	2 943	3465	21^1; 7^3	5155
4174	25^2; 21^1; 7^1	7 845	3603	21^1; 11^1; 7^2	3244
4260	25^3; 7^1	21 770	3644	29^1; 13^1; 7^1	4391
4321	25^1; 21^1; 7^3	5 451	3701	21^1; 13^1; 7^2	5010
4408	25^2; 7^3	14 910	3890	29^1; 21^1; 7^1	5677
4532	25^2; 10^1; 7^2	7 299	3946	21^2; 7^2	3508
4699	25^3; 21^1	4 404	4155	29^1; 7^3	4234
4705	25^2; 18^1; 7^2	4 311	4390	29^1; 13^1; 7^2	3743
4785	25^4	8 079	4447	21^1; 13^1; 7^3	2580
4846	25^2; 21^1; 7^2	10 640			
4932	25^3; 7^2	30 650			

[a]Sequential with increasing frequency.
[b]Molar absorption coefficient dm^3 mol^{-1} cm^{-1}.

different ionic state sequences by symmetry, both assignments show significant agreement with KT predictions. The PES analysis in Tables IV and V shows 13 ionic states for NBD where the loss of electronic charge density on ionization is almost entirely confined to a single configuration; this is much higher than for QC, where only eight ionic states have a high pole strength (intensity) over 0.8. Both indicate that ionization proceeds without a major structural change; the low reorganization energy probably arises from the rigidity of these cage-like structures. The NBD and QC difference is a direct result of the π-electron system in NBD where many of the shake-up states have $\pi\pi^*$ excitations accompanying the ionization. For QC, where π-electrons are absent, the corresponding $\sigma\sigma^*$ excitations occur at significantly higher energies.

D. Vibrationally excited states

1. Norbornadiene

All previous photoelectron studies of NBD and QC[17–24] observed the lowest IE as a single band rather than the multiplet shown in Fig. 3 for NBD and in Fig. 5 for QC. The adiabatic ionization energy (AIE_1) for NBD, assigned to the $^2B_1$ state at 8.279 eV, shows this progression of 18 members, with decreasing vibration frequency from 392 cm^{-1} to 340 cm^{-1}; our calculated frequency for the $^2B_1$ state at the MP4(SDQ) level is 381 cm^{-1}. We correlate the Franck–Condon (FC) envelope of IE_1 with the NBD spectrum in Fig. 3. The envelope becomes progressively more complex with increasing energy, and a portion of this is shown in the supplementary material as Fig. SM6. Only a_1 vibrations contribute in this FC study, and these are summarized in Tables VI and VII; other vibrations of the b_1, b_2, and a_2 symmetry are shown in the supplementary material as Table SM6.

2. Quadricyclane

We find the AIE_1 for QC at 7.671 eV and assign it to the $^2B_2$ state. Our calculated vibration frequency for this state is 663 cm^{-1}. A weak vibrational progression of nine or more members with vibration frequency decreasing from 703 cm^{-1} to 660 cm^{-1} is evident on the leading edge of IE_1 of QC in Fig. 5 but with a clearly different vibrational separation from another series on the trailing edge. Thus, the minor contamination of the QC sample by NBD makes it clear that the two sets of vibrations are unrelated. We have enhanced the differences by peak fitting and subtracting broad Gaussian peaks from the IE_1 band in Fig. 5 and processing the resulting regular residuals from the subtraction, as shown in Fig. 10. A summary of the calculated a_1 vibration frequencies and leading terms in the Franck–Condon analyses for the $^2B_2$ state is given in Tables VIII and IX, respectively.

The full Franck–Condon analysis is superimposed on the initial band of the QC PES in Fig. 11. The calculated envelope gives a realistic account of the leading edge of the spectrum.

The next two ionizations for QC are the strongly overlapping doublet, centered on 10 eV, which we attribute to $^2A_2 \leq {}^2B_1$. We have performed a fit of the observed PES using two separate Gaussian functions, as shown in the supplementary material under SM3(c). The difference between the fitted functions and the PES is very
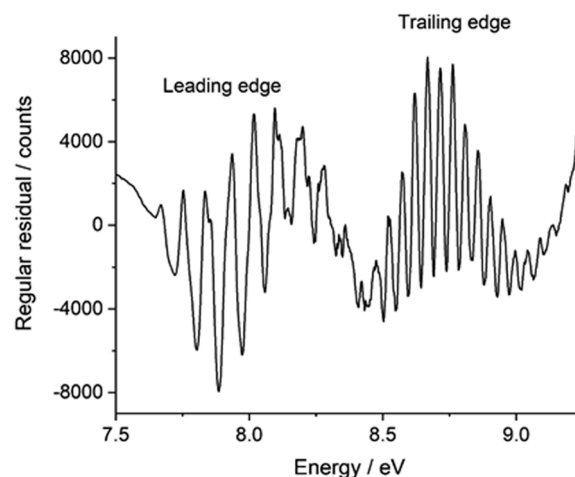

FIG. 10. The resulting regular residuals after a best fit asymmetric Gaussian function to the QC PES first band. The previously mentioned minor contamination of the sample by NBD is seen on the trailing edge with a quite different vibrational appearance occurring on the leading edge.

TABLE VIII. The a_1 harmonic frequencies including their sequence numbers for the ground and ionic states for quadricyclane determined at the TZVP level. The full sequences are shown in the supplementary material as SM6. The modes labeled in ascending frequency are the same as the Franck–Condon profiles of active modes shown in Table IX.

X^1A_1	$^2B_1$	$^2B_2$	$^2A_1$	$^2A_2$
6	2	5	7	6
744	716	663	714	732
8	7	8	9	9
825	782	765	797	830
12	8	12	12	15
932	870	898	870	974
15	13	13	15	17
975	885	946	931	993
17	17	18	17	18
1022	1005	1066	1 006	1035
22	19	20	23	22
1112	1055	1092	11 511 096	1190
28	23	28	27	25
1290	1220	1354	1 284	1273
29	26	29	28	29
1381	1303	1397	1 307	1379
31	29	31	31	30
1509	1409	1511	1 484	1517
32	29	32	32	31
3085	2936	3127	3 062	3110
35	36	35	37	36
3237	3256	3260	3 273	3249
39	39	39	39	38
3270	3269	3290	3 288	3258

TABLE IX. Vibrationally excited states for the $^2B_2$ state of quadricyclane using Franck–Condon methods. Energy of the 0–0 transition: 60 422 cm^{-1}. The modes excited shown here are the a_1 frequencies for the ionic state shown, together with the number (n) of quanta excited as "^n." Binary and higher combination bands are separated by semicolons.

Energy cm^{-1}	Modes excited + quanta	Relative intensity	Energy cm^{-1}	Modes excited + quanta	Relative intensity
0	0	897	2 393	18^1; 5^2	2 526
663	5^1	2 513	2 460	12^2; 5^1	13 640
765	8^1	287	2 494	18^1; 8^1; 5^1	340
898	12^1	2 604	2 561	12^2; 8^1	1 350
1066	18^1	276	2 627	18^1; 12^1; 5^1	3 461
1327	5^2	5 187	2 654	5^4	6 118
1354	28^1	243	2 681	28^1; 5^2	1 884
1428	8^1; 5^1	1 285	2 695	12^3	2 598
1562	12^1; 5^1	10 640	2 724	29^1; 5^2	549
1663	12^1; 8^1	690	2 729	18^1; 12^1; 8^1	280
1729	18^1; 5^1	1 214	2 755	8^1; 5^3	3 634
1797	12^2	3 374	2 779	5^3; 1^2	306
1964	18^1; 12^1	795	2 782	28^1; 8^1; 5^1	322
1990	5^3	6 721	2 795	18^2; 5^1	229
2017	28^1; 5^1	985	2 856	8^2; 5^2	487
2061	29^1; 5^1	273	2 862	18^1; 12^2	1 023
2092	8^1; 5^2	2 725	2 889	12^1; 5^3	24 790
2116	5^2; 1^2	241	2 916	28^1; 12^1; 5^1	2 594
2193	8^2; 5^1	221	2 959	29^1; 12^1; 5^1	670
2225	12^1; 5^2	20 520	2 990	12^1; 8^1; 5^2	6 434
2252	28^1; 12^1	647	3 014	12^1; 5^2; 1^2	580
2296	29^1; 12^1	159	2 393	18^1; 5^2	2 526
2326	12^1; 8^1; 5^1	3 065	2 460	12^2; 5^1	13 640
2351	12^1; 5^1; 1^2	291	2 494	18^1; 8^1; 5^1	340

small and largely confined to the onset and trailing edges. This is where spectral interactions with adjacent peaks become relevant and also where the anharmonicity of the PES states is neglected in the fit. The two ionizations are separated, experimentally for VIE and
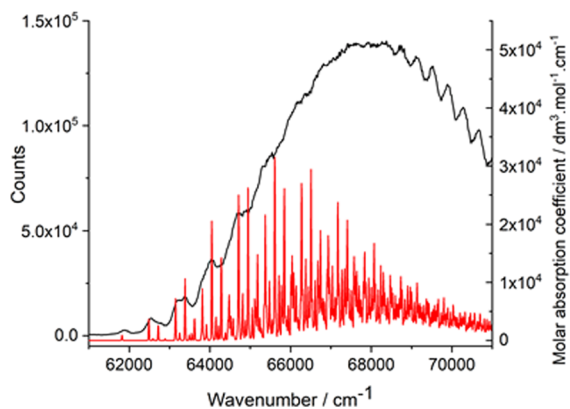

FIG. 11. The quadricyclane IE$_1$ $^2B_2$ state PES with the calculated Franck–Condon cold band structure superimposed.

theoretically for 0^0 bands, by 2726 cm^{-1} and 2904 cm^{-1}, respectively. The Gaussian simulation widens the VIE to 9.73 ± 0.05 eV and 10.25 ± 0.05 eV, a separation of 4194 cm^{-1}. A summary of the lowest calculated vibrational states given in Table X is superimposed on the two simulations. Those shown in red have half-widths at half-maximum (HWHMs) (bandwidths) of 10 cm^{-1}. In both spectra, there are no vibrational spectral features visible. Tables IX and X show that several vibrational states are present in this small interval, making recognition of features in the spectrum impossible at this resolution. We have noted previously[87] that when two or more PES ionizations overlap, the effect is to degrade the spectral resolution of the higher energy one(s), owing to the interference between the vibrational wave-trains of the lower IE and the higher IE. In short, the two ionic states are strongly coupled, and conical intersections lie between their minima, an observation first made by Baldea et al.[88,89] in a study of the PhF ionic states. Without directly including the inter-state vibronic coupling in our previous simulations, we found that the smaller the separation of two ionic states, the larger the bandwidth of the fitting functions to the vibrational states necessary to achieve a match to experiment.[87] The bandwidth used in Fig. 12 has been widened to a HWHM of 400 cm^{-1} in blue to match the nearly featureless IE.

TABLE X. The low-lying vibrationally excited states of the $^2A_2$ and $^2B_1$ ionic states for quadricyclane. The modes excited shown here are the a_1 frequencies for the ionic state shown together with the number (n) of quanta excited as "^n." Binary and higher combination bands are separated by semicolons.

$^2A_2$ energy 0–0 transition: 75 188 cm^{-1}			$^2B_1$ energy 0–0 transition: 78 092 cm^{-1}		
Energy cm^{-1}	Modes excited + quanta	Relative intensity	Energy cm^{-1}	Modes excited + quanta	Relative intensity
0	0	14 110	0	0	99 620
486	1^2	1 032	657	1^2	1 054
556	2^2	225	716	5^1	13 670
732	5^1	25 510	736	2^1; 1^1	610
830	8^1	1 092	782	8^1	808
974	14^1	1 937	815	2^2	5 577
993	16^1	14 220	870	11^1	95 800
1190	21^1	13 070	885	13^1	27 880
1217	5^1; 1^2	2 528	947	3^2	283
1273	24^1	1 820	1005	17^1	4 522
1288	5^1; 2^2	512	1055	19^1	33 310
1463	5^2	18 700	1078	7^1; 1^1	732
1478	16^1; 1^2	977	1220	23^1	16 060
1549	16^1; 2^2	215	1303	26^1	17 950
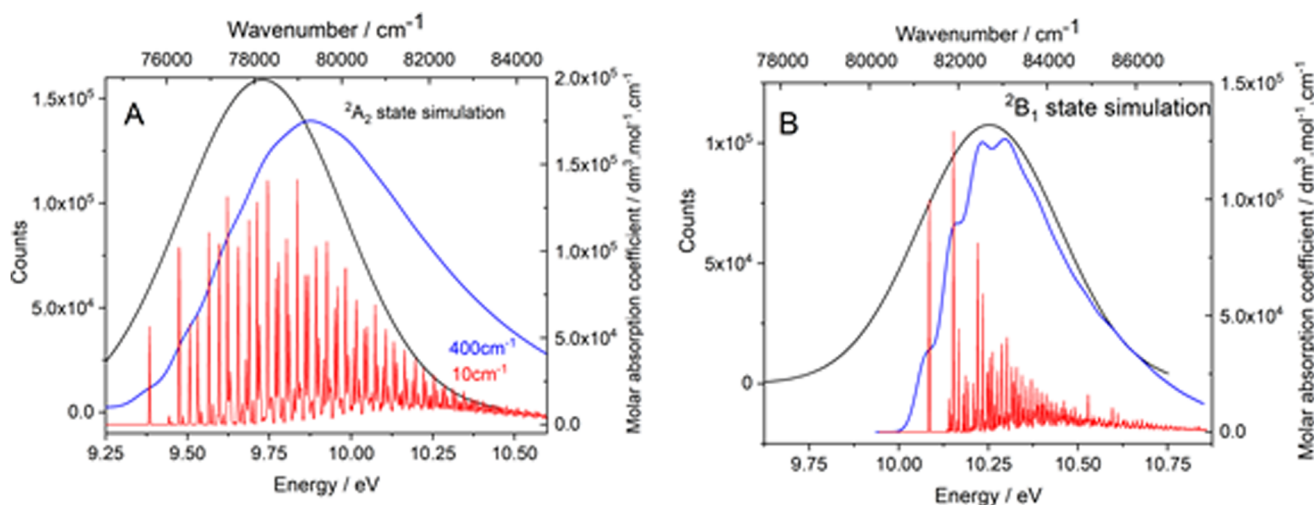
FIG. 12. The combined quadricyclane $^2A_2$ (A) and $^2B_1$ (B) states separated by two Gaussian fits. These two bands strongly overlap in the observed PES, and their separation is discussed in the text. The cold band structure calculated by Franck–Condon methods is shown in red; the individual lines that have half-widths at half-maximum of 10 cm^{-1} have been widened to HWHM of 400 cm^{-1} in blue.

IV. CONCLUSIONS

Our synthesis of QC showed that the previously accepted ^1H NMR coupling constants[27–31] could not interpret the 300 MHz spectrum; revised values were obtained by GIAO methods that show backward compatibility with both 60 MHz and 100 MHz spectra. The QC spectrum at 300 MHz shows that second order effects are still present for both NBD and QC, but especially for QC. We have theoretically determined the spin–spin coupling constants for QC in which all ^1H nuclei are coupled, and the spin coupling constants for symmetry related atoms are determined. These expose the weakness of simple (first order) analyses, where only coupling between chemically distinct atoms is considered and evaluated; this leads to the observed first order coupling constants being sums of constants rather than individual values.[31]

Our synchrotron-based photoelectron spectra of NBD and QC show the vibrational structure on the lowest IE in each case. NBD shows a vibrational progression of 18 members where the vibration frequency (ν) declines from 390 cm^{-1} to 340 cm^{-1} with an energy increase. Similarly, the lowest PES band for QC shows a vibrational progression of at least nine members but with ν decreasing from 703 cm^{-1} to 660 cm^{-1}.

The lowest AIEs of each symmetry were determined by MP4(SDQ) methods for each molecule. The adiabatic IE for NBD is assigned to the $^2B_1$ state with a_1 symmetry calculated frequency (381 cm^{-1}). In contrast, for QC, it is assigned to the $^2B_2$ state; here, the a_1 symmetry vibration frequency is calculated at 663 cm^{-1}. The AIE sequences are $^2B_1 < ^2A_1 < ^2A_2 < ^2B_2$ for NBD and $^2B_2 < ^2A_2 < ^2B_1 < ^2A_1$ for QC. The symmetry sequences of ionic states are the same for MP2 and MP4 methods for the respective molecules.

For both NBD and QC, the overall PES vertical ionization energy (VIE) profiles from onset to 20 eV for both compounds were closely reproduced by the Tamm–Dancoff approximation (TDA) both in energies and intensities.

The vibrational structure within the lowest AIE for each of NBD and QC, determined by Franck–Condon methods, gave a good account of the observed spectra. However, the observed multiplets for IE$_1$ in both cases show that the envelope consists of a complex set of vibrations, rather than as single progressions. We have presented theoretical PES envelopes that include vibrational states for some higher ionizations, but the prospects for experimentally detecting these will require a different technique than conventional PES since there is a substantial overlap between states of different symmetries, especially for QC. We have fitted two Gaussian functions to the combined $^2A_2 + ^2B_1$ states observed as a strongly overlapping doublet. The separated functions, after allowance for the lack of anharmonicity, and the effects of nearby ionizations on the leading and trailing edges give a reasonable interpretation of the band. We are unable to perform the Franck–Condon analysis on the separate $^2A_1$ state PES band since the software available to us is limited to a single negative vibration frequency. At the MP2, MP4, and MP4(SDQ) levels, the $^2A_1$ state generates three such values.

SUPPLEMENTARY MATERIAL

See the supplementary material for additional information on each of the following: (1) synthesis of quadricyclane, (2) the GAIO calculated ^1H and ^{13}C magnetic shielding and spin–spin coupling constants, (3) fits to the lowest two ionization energies for norbornadiene and quadricyclane and the combined third state of QC, (4) the ground state equilibrium structures of NBD and QC, (5) vibration frequencies of the ground and ionic states, (6) comparison of the molecular structures of NBD and QC with experimental microwave and other spectral data, and (7) bond and ring critical points.

APPENDIX

In order to maintain the focus on ionization in the main paper above, we include results and discussion of structural features here. A comparison of the experimental rotational constants with the present study is shown in Tables XI and XII. Rotational constants (A, B, C) give a relative measure of the overall shape via the moments of inertia. The CCSD(T) data show very close RC values for both NBD[68] and QC,[71] which differ from the MW data by less than 1%. The results from the MP4(SDQ) ground state calculations differ from the experimental data by a further small amount. The ground state structures of both NBD and QC determined by CCSD(T) procedures were very similar to those from fourth order Møller–Plesset perturbation theory, which included single double and quadruple excitations [MP4(SDQ)]. Fortunately, both were very similar to those from second order MP2 theory. In the case of NBD, there is a further close structural similarity with calculations that included triples [MP4(SDTQ)], but these calculations[38] appear to be more demanding than the CCSD(T) method itself.

TABLE XI. Comparison of rotational constants (A, B, C) of the X^1A_1 equilibrium structure with the lowest ionic states of each symmetry for NBD in the microwave substitution structure at the MP4(SDQ) level.

	Norbornadiene						
	X^1A_1	X^1A_1	X^1A_1	$^2B_1$	$^2A_1$	$^2B_2$	$^2A_2$
Method	MW[65]	CCSD(T)	MP4(SDQ)	MP4(SDQ)	MP4(SDQ)	MP4(SDQ)	MP4(SDQ)
Energy (eV)				0.0	8.185	9.183	10.607	10.998
Bond C_1–C_2 (Å)	...	1.5387	1.5387	1.5202	1.5072	1.5284	1.6083
Bond C_2=C_3 (Å)	...	1.3368	1.3367	1.3770	1.3633	1.3315	1.2999
Bond C_1–C_7 (Å)	...	1.5520	1.5520	1.5443	1.6154	1.6527	1.5417
A (MHz)	4273.628(1)	4279.484	4315.7355	3988.6715	4410.9638	4233.4797	4137.4251
B (MHz)	3610.300(1)	3611.745	3617.8461	3849.1624	3654.6405	3406.5428	3493.2552
C (MHz)	3186.437(1)	3182.315	3184.0941	3473.6487	3024.1345	3190.4099	3186.4828

TABLE XII. Structural details of QC in the ground X^1A_1 equilibrium structure and first ionic states of each symmetry, calculated rotational constants (A, B, C), determined at the MP4(SDQ) level.

	Quadricyclane						
	X^1A_1	X^1A_1	X^1A_1	$^2B_2$	$^2A_2$	$^2B_1$	$^2A_1$
Method	MW[67]	CCSD(T)	MP4(SDQ)	MP4(SDQ)	MP4(SDQ)	MP4(SDQ)	MP4(SDQ)
Energy (eV)			0.0	7.482	9.185	9.757	10.634
Bond C_1–C_2 (Å)	. . .	1.5217	1.5143	1.4977	1.5993	1.5421	1.4846
Bond C_2–C_6 (Å)	. . .	1.5187	1.5458	1.4756	1.5059	1.6462	1.6015
Bond C_1–C_7 (Å)	. . .	1.5149	1.5139	1.5356	1.5027	1.4836	1.5509
A (MHz)	4408.2184(2)	4406.271	4426.9300	4384.8284	4492.9622	4381.1570	4575.2727
B (MHz)	4345.5142(2)	4347.729	4368.0907	4260.3649	4216.3741	4321.8614	4059.4725
C (MHz)	3256.2893(2)	3256.391	3267.6349	3427.2813	3161.8450	3123.9866	3266.8885

In all our methods, the rotational constants, centrifugal distortion constants, and dipole moments are very close to microwave values. We believe that this is not accidental but demonstrates the quality of the studies; this leads to confidence in the ionic state study.

DATA AVAILABILITY

The data that support the findings of this study and its supplementary material are available from the corresponding author upon reasonable request.

REFERENCES

[1] M. H. Palmer, M. Coreno, M. de Simone, C. Grazioli, S. V. Hoffmann, and N. C. Jones, J. Chem. Phys. **150**, 194305 (2019).

[2] M. H. Palmer, R. A. Aitken, M. Coreno, M. de Simone, C. Grazioli, S. V. Hoffmann, and N. C. Jones, J. Chem. Phys. **152**, 144301 (2020).

[3] M. H. Palmer, S. V. Hoffmann, N. C. Jones, M. Coreno, M. de Simone, and C. Grazioli, J. Chem. Phys. **151**, 084304 (2019).

[4] M. H. Palmer, S. V. Hoffmann, N. C. Jones, M. Coreno, M. de Simone, C. Grazioli, and R. A. Aitken, J. Chem. Phys. **153**, 054301 (2020).

[5] U. Bauer, L. Fromm, C. Weiß, P. Bachmann, F. Späth, F. Düll, J. Steinhauer, W. Hieringer, A. Görling, A. Hirsch, H.-P. Steinrück, and C. Papp, J. Phys. Chem. C **123**, 7654–7664 (2019).

[6] U. Bauer, L. Fromm, C. Weiß, F. Späth, P. Bachmann, F. Düll, J. Steinhauer, S. Matysik, A. Pominov, A. Görling, A. Hirsch, H.-P. Steinrück, and C. Papp, J. Chem. Phys. **150**, 184706 (2019).

[7] O. Brummel, F. Waidhas, U. Bauer, Y. Wu, S. Bochmann, H.-P. Steinrück, C. Papp, J. Bachmann, and J. Libuda, J. Phys. Chem. Lett. **8**, 2819–2825 (2017).

[8] C. Philippopoulos, D. Economou, C. Economou, and J. Marangozis, Ind. Eng. Chem. Prod. Res. Dev. **22**, 627–633 (1983).

[9] B. E. Tebikachew, H. B. Li, A. Pirrotta, K. Börjesson, G. C. Solomon, J. Hihath, and K. Moth-Poulsen, J. Phys. Chem. C **121**, 7094–7100 (2017).

[10] B. E. Tebikachew, F. Edhborg, N. Kann, B. Albinsson, and K. Moth-Poulsen, Phys. Chem. Chem. Phys. **20**, 23195–23201 (2018).

[11] M. Quant, A. Lennartson, A. Dreos, M. Kuisma, P. Erhart, K. Börjesson, and K. Moth-Poulsen, Chem. - Eur. J. **22**, 13265–13274 (2016).

[12] A. Cuppoletti, J. P. Dinnocenzo, J. L. Goodman, and I. R. Gould, J. Phys. Chem. A **103**, 11253–11256 (1999).

[13] M. Bertram, F. Waidhas, M. Jevric, L. Fromm, C. Schuschke, M. Kastenmeier, A. Görling, K. Moth-Poulsen, O. Brummel, and J. Libuda, J. Chem. Phys. **152**, 044708 (2020).

[14] A. Dreos, Z. Wang, B. E. Tebikachew, K. Moth-Poulsen, and J. Andréasson, J. Phys. Chem. Lett. **9**, 6174–6178 (2018).

[15] M. Quant, A. Hamrin, A. Lennartson, P. Erhart, and K. Moth-Poulsen, J. Phys. Chem. C **123**, 7081–7087 (2019).

[16] P. Bischof, J. A. Hashmall, E. Heilbronner, and V. Hornung, Helv. Chim. Acta **52**, 1745–1749 (1969).

[17] D. A. Demeo and A. J. Yencha, J. Chem. Phys. **53**, 4536–4543 (1970).

[18] E. Heilbronner and H.-D. Martin, Helv. Chim. Acta **55**, 1490–1502 (1972).

[19] E. Lindholm, C. Fridh, and L. Åsbrink, Faraday Discuss. Chem. Soc. **54**, 127–138 (1972).

[20] K. Ohno, T. Ishida, Y. Naitoh, and Y. Izumi, J. Am. Chem. Soc. **107**, 8082–8086 (1985).

[21] G. Bieri, F. Burger, E. Heilbronner, and J. P. Maier, Helv. Chim. Acta **60**, 2213–2233 (1977).

[22] H. D. Roth and M. L. M. Schilling, J. Am. Chem. Soc. **103**, 7210–7217 (1981).

[23] K. Ishiguro, I. V. Khudyakov, P. F. McGarry, N. J. Turro, and H. D. Roth, J. Am. Chem. Soc. **116**, 6933–6934 (1994).

[24] R. D. Bach, I. L. Schilke, and H. B. Schlegel, J. Org. Chem. **61**, 4845–4847 (1996).

[25] Y. Inadomi, K. Morihashi, and O. Kikuchi, J. Mol. Struct.: THEOCHEM **434**, 59–66 (1998).

[26] See https://webbook.nist.govcgicbook.cgi?ID=C121460&Mask=20#Ion-Energetics and https://webbook.nist.govcgicbook.cgi?ID=C278068&Mask=69 for NIST Chemistry WebBook SRD 69.

[27] R. Radeglia, H. Poleschner, and G. Haufe, Magn. Reson. Chem. **31**, 639–641 (1993).

[28] W. Offermann, Magn. Reson. Chem. **20**, 203–204 (1982).

[29] T. Parella, F. Sánchez-Ferrando, and A. Virgili, Magn. Reson. Chem. **33**, 196–200 (1995).

[30] R. Hübers, M. Klessinger, and K. Wilhelm, Magn. Reson. Chem. **24**, 1016–1019 (1986).

[31] P. Laszlo and P. V. R. Schleyer, J. Am. Chem. Soc. **86**, 1171–1179 (1964).

[32] C. D. Smith, Org. Synth. **51**, 133–135 (1971).

[33] G. S. Hammond, N. J. Turro, and A. Fischer, J. Am. Chem. Soc. **83**, 4674–4675 (1961).

[34] W. G. Dauben and R. L. Cargill, Tetrahedron **15**, 197–201 (1961).

[35] L. Pan, R. Feng, H. Peng, E. Xiu-Tian-Feng, J.-J. Zou, L. Wang, and X. Zhang, RSC Adv. **4**, 50998–51001 (2014).

[36] O. Baumgärtel and G. Szeimies, Chem. Ber. **116**, 2180–2204 (1983).

[37] P. L. Beaulieu, A. Kabo, and D. G. Garratt, Can. J. Chem. **58**, 1014–1020 (1980).

[38] M. J. Frisch, G. W. Trucks, H. B. Schlegel, G. E. Scuseria, M. A. Robb, J. R. Cheeseman, G. Scalmani, V. Barone, G. A. Petersson, H. Nakatsuji, X. Li, M. Caricato, A. V. Marenich, J. Bloino, B. G. Janesko, R. Gomperts, B. Mennucci, H. P. Hratchian, J. V. Ortiz, A. F. Izmaylov, J. L. Sonnenberg, D. Williams-Young, F. Ding, F. Lipparini, F. Egidi, J. Goings, B. Peng, A. Petrone, T. Henderson, D. Ranasinghe, V. G. Zakrzewski, J. Gao, N. Rega, G. Zheng, W. Liang, M. Hada, M. Ehara, K. Toyota, R. Fukuda, J. Hasegawa, M. Ishida, T. Nakajima, Y. Honda, O. Kitao, H. Nakai, T. Vreven, K. Throssell, J. A. Montgomery, Jr., J. E. Peralta, F. Ogliaro, M. J. Bearpark, J. J. Heyd, E. N. Brothers, K. N. Kudin, V. N. Staroverov, T. A. Keith, R. Kobayashi, J. Normand, K. Raghavachari, A. P. Rendell, J. C. Burant, S. S. Iyengar, J. Tomasi, M. Cossi, J. M. Millam, M. Klene, C. Adamo, R. Cammi, J. W. Ochterski, R. L. Martin, K. Morokuma, O. Farkas, J. B. Foresman, and D. J. Fox, Gaussian 16 Revision A.03, Gaussian Inc., Wallingford, CT, 2016.

[39] H.-J. Werner, P. J. Knowles, F. R. Manby, M. Schütz, P. Celani, T. Korona, R. Lindh, A. Mitrushenkov, G. Rauhut, K. R. Shamasundar, T. B. Adler, R. D. Amos, A. Bernhardsson, A. Berning, D. L. Cooper, M. J. O. Deegan, A. J. Dobbyn, F. Eckert, E. Goll, C. Hampel, A. Hesselmann, G. Hetzer, T. Hrenar, G. Jansen, C. Köppl, Y. Liu, A. W. Lloyd, R. A. Mata, A. J. May, S. J. McNicholas, W. Meyer, M. E. Mura, A. Nicklaß, D. P. O'Neill, P. Palmieri, K. Pflüger, R. Pitzer, M. Reiher, T. Shiozaki, H. Stoll, A. J. Stone, R. Tarroni, T. Thorsteinsson, M. Wang, and A. Wolf, MOLPRO Version 2012.1, A package of *ab initio* programs, 2012; see https://www.molpro.net.

[40] H. J. Werner and P. J. Knowles, J. Chem. Phys. **82**, 5053–5063 (1985).

[41] M. J. Frisch, M. Head-Gordon, and J. A. Pople, Chem. Phys. Lett. **166**, 275–280 (1990).

[42] M. J. Frisch, M. Head-Gordon, and J. A. Pople, Chem. Phys. Lett. **166**, 281–289 (1990).

[43] G. D. Purvis III and R. J. Bartlett, J. Chem. Phys. **76**, 1910–1918 (1982).

[44] S. J. Cole and R. J. Bartlett, J. Chem. Phys. **86**, 873–881 (1987).

[45] R. Krishnan and J. A. Pople, Int. J. Quantum Chem. **14**, 91–100 (1978).

[46] G. W. Trucks, J. D. Watts, E. A. Salter, and R. J. Bartlett, Chem. Phys. Lett. **153**, 490–495 (1988).

[47] G. W. Trucks, E. A. Salter, C. Sosa, and R. J. Bartlett, Chem. Phys. Lett. **147**, 359–366 (1988).

[48] J. Schirmer and L. S. Cederbaum, J. Phys. B: At. Mol. Phys. **11**, 1889–1900 (1978).

[49] I. H. Hillier, M. A. Vincent, M. F. Guest, and W. von Niessen, Chem. Phys. Lett. **134**, 403–406 (1987).

[50] M. F. Guest, I. J. Bush, H. J. J. Van Dam, P. Sherwood, J. M. H. Thomas, J. H. Van Lenthe, R. W. A. Havenith, and J. Kendrick, Mol. Phys. **103**, 719–747 (2005).

[51] V. Barone, J. Bloino, M. Biczysko, and F. Santoro, J. Chem. Theory Comput. **5**, 540–554 (2009).

[52] J. Bloino, M. Biczysko, F. Santoro, and V. Barone, J. Chem. Theory Comput. **6**, 1256–1274 (2010).

[53] A. Baiardi, J. Bloino, and V. Barone, J. Chem. Theory Comput. **9**, 4097–4115 (2013).

[54] J. R. Cheeseman, G. W. Trucks, T. A. Keith, and M. J. Frisch, J. Chem. Phys. **104**, 5497–5509 (1996).

[55] K. Wolinski, J. F. Hinton, and P. Pulay, J. Am. Chem. Soc. **112**, 8251–8260 (1990).

[56] R. Ahlrichs and P. R. Taylor, J. Chim. Phys. **78**, 315–324 (1981).

[57] P. C. Hariharan and J. A. Pople, Theor. Chim. Acta **28**, 213–222 (1973).

[58] F. Weigend, Phys. Chem. Chem. Phys. **8**, 1057–1065 (2006).

[59] V. Barone, in *Recent Advances in Density Functional Methods, Part I*, edited by D. P. Chong (World Scientific Publishing Company, Singapore, 1996) [Chemistry **1**, 287–334 (1995)].

[60] V. Barone and S. Fliszár, J. Mol. Struct.: THEOCHEM **369**, 29–37 (1996).

[61] A. Yokozeki and K. Kuchitsu, Bull. Chem. Soc. Jpn. **44**, 2356–2363 (1971).

[62] Y. Morino, K. Kuchitsu, and A. Yokozeki, Bull. Chem. Soc. Jpn. **40**, 1552 (1967).

[63] L. Doms, H. J. Geise, C. Van Alsenoy, L. Van den Enden, and L. Schäfer, J. Mol. Struct. **129**, 299–314 (1985).

[64] J. W. Emsley and J. C. Lindon, Mol. Phys. **29**, 531–538 (1975).

[65] K. C. Cole and D. F. R. Gilson, J. Mol. Struct. **82**, 71–75 (1982).

[66] W. A. Heeschen, D. W. Alderman, and D. M. Grant, J. Phys. Chem. **92**, 6504–6511 (1988).

[67] G. Knuchel, G. Grassi, B. Vogelsanger, and A. Bauder, J. Am. Chem. Soc. **115**, 10845–10848 (1993).

[68] B. Vogelsanger and A. Bauder, J. Mol. Spectrosc. **130**, 249–257 (1988).

[69] J. Demaison, J. Vogt, and G. Wlodarczak, "Rotational and related constants of diamagnetic asymmetric top molecules," in *1. Introduction: Landolt-Börnstein—Group II Molecules and Radicals*, Rotational and Related Constants of Diamagnetic Asymmetric Top Molecules Vol. 19B, edited by W. Hüttner (Springer-Verlag Berlin Heidelberg, 1992).

[70] B. Vogelsanger and A. Bauder, J. Mol. Spectrosc. **136**, 62–67 (1989).

[71] C. Aroulanda, P. Lesot, D. Merlet, and J. Courtieu, J. Phys. Chem. A **107**, 10911–10918 (2003).

[72] D. W. Rogers and F. J. McLafferty, J. Phys. Chem. A **103**, 8733–8737 (1999).

[73] K. Raghavachari, R. C. Haddon, and H. D. Roth, J. Am. Chem. Soc. **105**, 3110–3114 (1983).

[74] I. W. Levin and W. C. Harris, "Interpretation of the vibrational spectra of bicyclic hydrocarbons: norbornane and norbornadiene," Spectrochim. Acta, Part A **29**, 1815–1834 (1973).

[75] R. T. Boeré, J. A. Eng, K. Preuss, M. Parvez, C. D. Bryan, and A. W. Cordes, Can. J. Chem. **72**, 1171–1180 (1994).

[76] L. B. Krivdin, Magn. Reson. Chem. **42**, 919–930 (2004).

[77] T. Enevoldsen, J. Oddershede, and S. P. A. Sauer, Theor. Chem. Acc. **100**, 275–284 (1998).

[78] R. Hoffmann, A. Imamura, and W. J. Hehre, J. Am. Chem. Soc. **90**, 1499–1509 (1968).

[79] R. Hoffmann, E. Heilbronner, and R. Gleiter, J. Am. Chem. Soc. **92**, 706–707 (1970).

[80] R. Hoffmann, Acc. Chem. Res. **4**, 1–9 (1971).

[81] T. Kobayashi, Phys. Lett. A **69**, 31–33 (1978).

[82] M. H. Kibel, M. K. Livett, and G. L. Nyberg, J. Electron Spectrosc. Relat. Phenom. **15**, 275–280 (1979).

[83] W. Von Niessen and G. H. F. Diercksen, J. Electron Spectrosc. Relat. Phenom. **16**, 351–357 (1979).

[84] M. H. Palmer, J. Mol. Struct. **161**, 333–345 (1987).

[85] H.-D. Martin, C. Heller, E. Haselbach, and Z. Lanyjova, Helv. Chim. Acta **57**, 465–472 (1974).

[86] E. Haselbach and H.-D. Martin, Helv. Chim. Acta **57**, 472–480 (1974).

[87] M. H. Palmer, T. Ridley, S. V. Hoffmann, N. C. Jones, M. Coreno, M. de Simone, C. Grazioli, M. Biczysko, and A. Baiardi, J. Chem. Phys. **142**, 134301 (2015).

[88] I. Baldea, J. Franz, P. G. Szalay, and H. Koppel, Chem. Phys. **65**, 329 (2006).

[89] E. Gindensperger, I. Bâldea, J. Franz, and H. Köppel, Chem. Phys. **338**, 207 (2007).

[90] See www.inmr.net for i-NMR Reader (version 6.1.7).

[91] See http:www.gnuplot.info for Gnuplot Release 5.0.7.

[92] Origin Version 2019 OriginLab Corporation, Northampton, MA, USA.

[93] R. Dennington, T. A. Keith, and J. M. Millam, GaussView version 6.1, Semichem Inc., Shawnee Mission, KS, 2016.

[94] See http:avogadro.cc for Avogadro: An open-source molecular builder and visualization tool, version 1.XX.